

Magnetic confinement of neutral atoms based on patterned vortex distributions in superconducting disks and rings

B. Zhang,^{1,2} M. Siercke,^{1,2} K.S. Chan,¹ M. Beian,^{1,2} M.J. Lim,³ and R. Dumke^{1,2,*}

¹*Division of Physics and Applied Physics, Nanyang Technological University, 21 Nanyang Link, Singapore 637371, Singapore*

²*Centre for Quantum Technologies, National University of Singapore, 3 Science Drive 2, Singapore 117543, Singapore*

³*Department of Physics, Rowan University, 201 Mullica Hill Road, Glassboro, NJ 08028, USA*

(Dated: October 3, 2018)

We propose and analyze neutral atom traps generated by vortices imprinted by magnetic field pulse sequences in type-II superconducting disks and rings. We compute the supercurrent distribution and magnetic field resulting from the vortices in the superconductor. Different patterns of vortices can be written by versatile loading field sequences. We discuss in detail procedures to generate quadrupole traps, self-sufficient traps and ring traps based on superconducting disks and rings. The ease of creating these traps and the low current noise in supercurrent carrying structures makes our approach attractive for designing atom chip interferometers and probes.

PACS numbers: 37.10.Gh, 03.75.Be, 74.78.Na

I. Introduction

Recently superconducting atom chips have generated a lot of interest due to their attractive properties, such as the Meissner effect for type-I superconductors and vortices for type-II superconductors [1–3]. Cold atoms have been trapped and manipulated near superconducting surfaces [3–5] and Bose-Einstein condensation (BEC) on a superconducting atom chip has been reported recently [6]. Thermal and technical noise in proximity to superconducting surfaces have been shown both theoretically and experimentally to be significantly reduced compared to conventional atom chips [7–14]. Superconducting atom chips have the potential to coherently interface atomic and molecular quantum systems with quantum solid state devices [15–19]. Furthermore, ultracold atoms can be used to probe properties of superconductors, such as the dynamics of vortices in type-II superconductors [20, 21].

Previously we reported on the design and realization of several types of magnetic traps involving linear type-II superconducting microstructures [22–24]. These traps are formed by the magnetic field carried by vortices imprinted in the superconductor to confine ultracold atoms. Loading of the vortices is accomplished by tailored external magnetic pulse sequences applied to the superconductor in the mixed state. In a different approach vortex-based magnetic traps have been observed after cooling a superconducting disk through the critical temperature in the presence of an external magnetic field [21].

In this article, we extend our investigation of vortex based microtrap geometries to type-II superconducting disks and rings. To this end we have developed a numerical approach to calculate the vortex patterns imprinted after applying various external magnetic field pulses to

the superconducting structure. Using this numerical approach we design quadrupole traps, self-sufficient traps and ring traps in the various superconducting geometries. We demonstrate that, by simple application of an additional bias field, a single quadrupole trap may be deformed into a ring. Considering the low current noise expected from the persistent supercurrents generating these traps, and the low thermal noise expected from superconducting atom chips, this method may be an attractive way to generate low-noise on-chip atom interferometry. Compared to other low noise traps generated by permanent magnets our system retains one desirable feature: The ability to control the trap parameters and geometry from shot to shot.

The paper is organized as follows. Sec. II describes the equations of motion for the sheet current density J in a type-II superconducting strip, disk and ring in an external magnetic field. To validate our numerical approach we compute the supercurrents in a superconducting strip, and compare them with analytical results [22]. For the two-dimensional structures considered in this paper no explicit analytical solution is known. In Sec. III we design several types of traps for cold atoms by tailoring the magnetic field pulses which induce vortex patterns in the superconducting disk and ring. Sec. IV summarizes our results.

II. Loading vortices

Consider a type-II thin superconducting strip, disk and ring in a magnetic field perpendicular to their surface (xy plane) as shown in fig.1. Here d denotes the thickness of the superconductors and a denotes the half width of the strip and the (outer) radius of the disk and ring. The strip is assumed to be infinitely long along y , so that we can restrict our simulation to the xz plane. Similarly, we can reduce our simulation to the rz plane for the disk and ring due to rotational symmetry. Throughout the paper

*Electronic address: rdumke@ntu.edu.sg

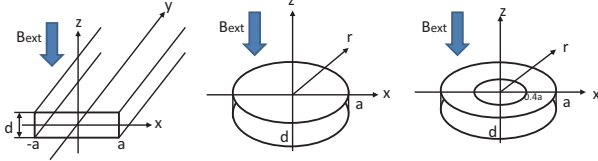


FIG. 1: (Color online) Schematic of the investigated type-II superconductor geometries. All geometries are assumed to be in the thin film limit with a thickness d . Shown are a strip of width $2a$ (left), a disk with radius a (center) and a ring with an outer radius of a and an inner radius of $0.4a$ (right). The magnetic field pulses are applied perpendicular to the surface.

we will assume that the temperature of the superconductors is below the critical value T_c and that the thickness d is small compared to the other length scales of the system. When the external field B_{ext} exceeds the lower critical field B_{c1} , but lies below the upper critical value B_{c2} , magnetic flux starts to penetrate the superconductor in the form of Abrikosov vortices [25]. To facilitate our numerical analysis we model these vortices together with the screening current as a macroscopic supercurrent $J(u, t)$. Our approach closely follows the method outlined in [26, 27] which makes use of the continuum approximation where the flux line spacing and the magnetic field penetration depth are small compared to all other relevant length scales considered [28]. From the distribution of the supercurrent we then compute the total magnetic field outside of the superconductor using the Biot-Savart law. We approximate the current density in the superconductor to be constant over its thickness d , which is valid in the thin-film approximation where d is smaller than the London penetration depth of the superconductor. The sheet current density is then defined as $J(x) = j(x)d$, where $j(x)$ is the local current density.

The perpendicular field component $B_z(x)$ generated in the specimen plane $z = 0$ by a constant B_{ext} and by the sheet current $J(x)$ along y for the strip can be written as [26]:

$$B_z(x) = B_{ext} + \frac{\mu_0}{2\pi} \int_0^a J(u) \left(\frac{1}{x-u} - \frac{1}{x+u} \right) du, \quad (1)$$

For cylindrically symmetric structures, where $J(r)$ is circling clockwise, we can write the perpendicular magnetic field component with $r_0 = 0$ for disks and $r_0 = 0.4a$ for rings as [26]:

$$B_z(r) = B_{ext} + \frac{\mu_0}{2\pi} \int_{r_0}^a J(u) \left(\frac{E(k)}{r-u} - \frac{K(k)}{r+u} \right) du, \quad (2)$$

where $E(k)$ and $K(k)$ are the first and second kind of the complete elliptic integrals with $k = \sqrt{4ru}/(r+u)$ and μ_0 is the vacuum permeability [26, 27]. In order to find an expression for the sheet current density $J(x)$ we take into account the time-dependence of B_{ext} and use Maxwell's equations, to arrive at the equation of motion

for the sheet current density $J(x, t)$ of the strip [26]:

$$J(x, t) = \tau \left[2\pi x \frac{dB_{ext}}{dt} + \int_0^a \frac{\partial J(u, t)}{\partial t} M(x, u) du \right], \quad (3)$$

and $J(r, t)$ for disks and rings [26]:

$$J(r, t) = \tau \left[\pi r \frac{dB_{ext}}{dt} + \int_{r_0}^a \frac{\partial J(u, t)}{\partial t} Q(r, u) du \right], \quad (4)$$

where

$$\begin{aligned} M(x, u) &= \ln \left| \frac{x-u}{x+u} \right|, \\ Q(r, u) &= -\frac{u}{r} \int_{r_0/u}^{r/u} \left(\frac{E(\frac{\sqrt{4\omega}}{1+\omega})}{1-\omega} + \frac{K(\frac{\sqrt{4\omega}}{1+\omega})}{1+\omega} \right) \omega d\omega, \\ \tau &= \frac{\mu_0 a d}{2\pi \rho(J)}. \end{aligned} \quad (5)$$

Here, $\rho(J) = \rho_c (J/J_c)^{n-1}$ is the nonlinear resistivity with critical value ρ_c , and $n = U_0/k_b T$ where U_0 is the characteristic activation energy of the superconductor [29]. J_c is the critical sheet current density [26, 27], defined as the maximum current density the superconductor can carry without a transition into the normal state. For the scope of this paper we have chosen the value of $n = 19$. This value gives a moderate response of the superconductor to applied fields. The exact value for n is material dependent and does not qualitatively alter the characteristic current distributions discussed for the experimentally applicable values.

We approximate the integration in Eq.3 and 4 by a Riemann Sum. First, we discretise the width of the strip and disk (or ring) into N elements with the same size $\Delta x = a/N$ or $\Delta r = a/N$ ($\Delta r = a - (r_0)/N$), and denote the middle point of each element by x_n or r_n , $n = 1, 2, \dots, N$. Then we rewrite Eq.3 in the form of a Riemann Sum in matrix form

$$J(x_i, t) = \tau \left[2\pi x_i \frac{dB_{ext}}{dt} + \sum_{j=1}^{j=N} M(x_i, x_j) \frac{\partial J(x_j, t)}{\partial t} \right]. \quad (6)$$

To solve the differential equation, we invert Eq.6 to find an equation for $\frac{\partial J(x_j, t)}{\partial t}$

$$\frac{\partial J(x_i, t)}{\partial t} = \sum_{j=1}^{j=N} M^{-1}(x_i, x_j) \left[\frac{J(x_j, t)}{\tau} - 2\pi x_j \frac{dB_{ext}}{dt} \right], \quad (7)$$

where $M^{-1}(x_i, x_j)$ is the inverse of the matrix $M(x_i, x_j)$. Now, we can use the Euler method and the initial conditions $J(x_i, t_0) = 0$ and $B_{ext}(t_0) = 0$ to compute the sheet

current density $J(x_i, t_n)$ at $t = t_n$ by

$$J(x_i, t_n) = \left(\sum_{j=1}^{j=N} M^{-1}(x_i, x_j) \left[\frac{J(x_j, t)}{\tau} - 2\pi x_j \frac{dB_{ext}}{dt} \right] + J(x_i, t_{n-1}) \right) \times \Delta t, \quad (8)$$

where $\Delta t = t_n - t_{n-1}$. The same approach can be used for Eq.4. From the above Eq.8, we can see that the final sheet current density $J(x_i, t_n)$ is only dependent on the initial conditions and t_n , not on dB_{ext}/dt . After we obtain $J(x_i, t_n)$, we compute the B field outside of the superconducting film ($z > 0$) using the Biot-Savart law.

In order to validate our numerical model, we consider the case of vortices induced in a superconducting strip, for which an analytical solution exists [22]. Applying a magnetic field pulse with a magnitude of B_{ext} perpendicular to the strip surface, the magnetic flux penetrates the strip. We solve Eq.3 numerically and obtain the distribution of supercurrents in the strip plotted in Fig.2 (solid lines). The small difference in the curves arises from the fact that the analytical solution assumes that at the edge, where the magnetic flux penetrates, the sheet current density takes the critical value. For the numerical computation the sheet current density is completely determined by Eq.3.

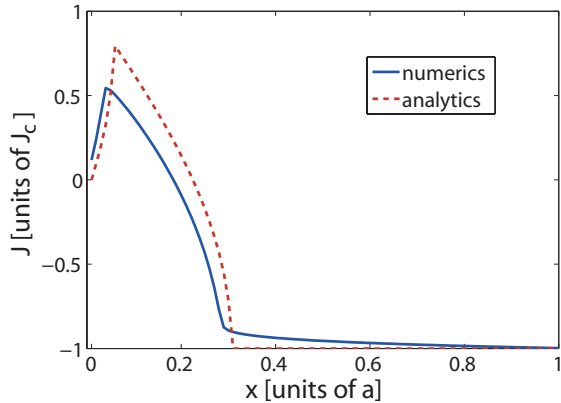


FIG. 2: (Color online) Distribution of the sheet current density across the strip for $B_{ext} = 0 \rightarrow \mu_0 J_c \rightarrow 0$. Solid line: sheet current density obtained by Eq.3; Dashed line: sheet current density our former results [22].

III. Magnetic traps

In this section, we apply Eq.4 to compute the sheet current density induced in the superconducting disk and ring by various loading fields. From the distribution of the sheet current density we then compute the magnetic field carried by the vortices by means of the Biot-Savart law. An intuitive picture of the vortex loading process

can be found in [30].

A. Traps generated by a superconducting disk

Consider a disk shaped superconductor in the remanent state with a magnetic loading field pulse of $B_{ext} = 0 \rightarrow 1.2\mu_0 J_c \rightarrow 0$. The second critical field in our calculations is approximately $1.8\mu_0 J_c$. For symmetry reasons the radial component of the total external field is always zero $B_r(r = 0, z) = 0$ above the disk center. The z component of the total external field $B_z(r = 0, z)$ above the disk center at different heights is plotted in Fig.3. $B_z(r, z)$ is always zero at the surface center of the disk ($r = 0, z = 0$), because the superconductor prevents any magnetic field perpendicular to its surface at this point. The inset of Fig.4 shows the supercurrent distribution obtained from Eq.4. We see that the supercurrent in the disk is separated into two regions; one with current propagating clockwise and one with current in the counter-clockwise direction. Applying a small bias field on the order of $B_{ext}/10$ perpendicular to the disk, allows us to cancel $B_z(r = 0, z = z_0)$ at z_0 and create a quadrupole trap for low-field seeking atoms. Fig.4 shows such a trap for $B_{bias} = -0.05\mu_0 J_c$ and $z_0 \sim 1.2a$. Increasing the bias field will move this trap closer to the disk surface, however in doing so the bias field will also induce currents into the disk, ensuring that the field at the disk surface center remains 0. This puts a J_c dependent limit on the trap depth for traps created very close to the disk surface.

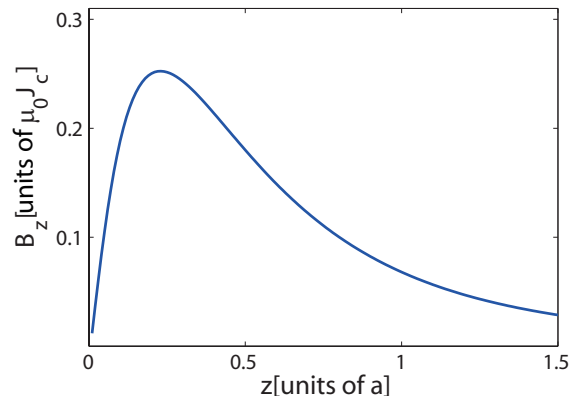


FIG. 3: (Color online) Vertical component $B_z(r, z)$ of the magnetic field carried by vortices loaded by $B_{ext} = 0 \rightarrow 1.2\mu_0 J_c \rightarrow 0$ vs z above the disk center $r = 0$.

The superconductor has a memory of the history of the external fields. Therefore it is possible to design a pulse sequence in which the role of the bias field is assumed by another induced supercurrent carried by the disk. Here we use two loading pulses with amplitudes of $0.8\mu_0 J_c$ and $-0.4\mu_0 J_c$ respectively to write a vortex pattern in the disk, which results in a self-sufficient trap

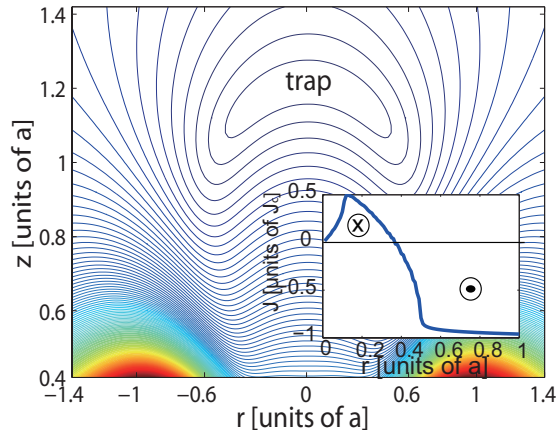


FIG. 4: (Color online) Equipotential lines showing a quadrupole trap above the disk center formed by the vortex field together with a perpendicular field $B_{bias} = -0.05\mu_0 J_c$. The vortex loading field pulse has an amplitude of $1.2\mu_0 J_c$. The field variation per contour line is $5 \times 10^{-3} \mu_0 J_c$. Inset: Distribution of the sheet current density along the radial direction resulting from the loading field pulse.

above the disk center, as shown in Fig.5. Choosing typical experimental values for the critical current density of YBCO at liquid Nitrogen temperatures $j_c = 1\text{MA}/\text{cm}^2$ we calculate a self-sufficient trap depth of $35\mu\text{K}$ for a disk with a diameter of 1mm. This trap has the feature of transforming into a ring trap by applying an additional perpendicular bias field $B_{bias} = 0.01\mu_0 J_c$.

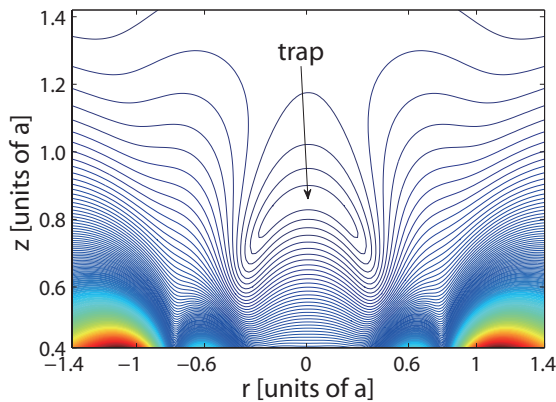


FIG. 5: (Color online) A self-sufficient trap above the disk center formed by the vortex field created by two loading field pulses with amplitudes $0.8\mu_0 J_c$ and $-0.4\mu_0 J_c$ respectively. The field variation per contour line is $9.5 \times 10^{-4} \mu_0 J_c$.

While it is possible to split the self-sufficient trap into a ring, it does not necessarily imply a simple loading procedure with a high transfer efficiency from an external trap via the self-sufficient trap. A more straightforward way of producing a ring trap from an external quadrupole trap is to use a first magnetic field pulse of $1.2\mu_0 J_c$ fol-

lowed by a second pulse $-0.6\mu_0 J_c$. Due to the nonlinear response of the material, this pulse sequence does not result in a self-sufficient trap, and instead a quadrupole trap can be formed far away from the chip surface by applying an additional bias field B_{bias} . By increasing the value of B_{bias} this trap is brought closer to the chip surface where it eventually deforms into a ring trap. The perpendicular bias field lifts the field zero on the

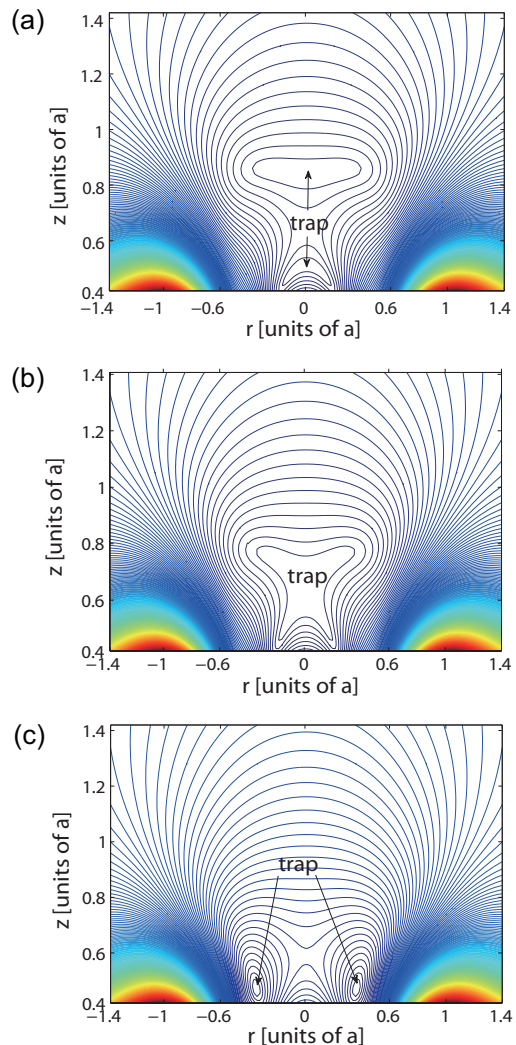


FIG. 6: (Color online) Equipotential lines for an atom with nonzero magnetic moment. The loading field pulses are $B_{ext} = 0 \rightarrow 1.2\mu_0 J_c \rightarrow -0.6\mu_0 J_c \rightarrow 0$. (a) With an additional bias field $B_{bias} = 0.03\mu_0 J_c$, two traps are obtained above the disk center. The field variation per contour line is $1.5 \times 10^{-3} \mu_0 J_c$. (b) $B_{bias} = 0.035\mu_0 J_c$, the two traps merge. The field variation per contour line is $1.54 \times 10^{-3} \mu_0 J_c$. (c) $B_{bias} = 0.06\mu_0 J_c$, a ring trap is formed. The field variation per contour line is $1.2 \times 10^{-3} \mu_0 J_c$.

disk surface and lowers the quadrupole trap, producing two traps above the disk center, see Fig.6(a). Increasing the bias field brings the two traps closer together, until they merge at $B_{bias} = 0.03\mu_0 J_c$, see Fig.6(b). Increas-

ing B_{bias} further will turn the trap into a ring trap, as shown in Fig.6(c). Continuing to increase B_{bias} increases the radius of the ring trap until the trap is lowered to the surface.

B. Traps generated by a superconducting ring

In this section we consider an annular superconductor. The inset of Fig.8(a) shows the supercurrents carried by the vortices in the remanent state, when we apply a field pulse with a magnitude of $0.8\mu_0J_c$ to a superconducting ring.

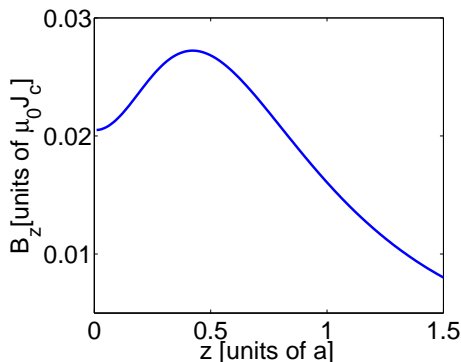


FIG. 7: (Color online) $B_z(r = 0, z)$ carried by the vortices at different z above the ring center. The loading field pulse is $B_{ext} = 0 \rightarrow 0.8\mu_0J_c \rightarrow 0$.

Similar to the superconducting disk, $B_r(r = 0, z)$ is always zero by symmetry. We plot the z component of the magnetic field $B_z(r = 0, z)$ generated by these supercurrents at different height z in Fig.7. If an additional perpendicular field is applied to cancel $B_z(r = 0, z = z_0)$, a quadrupole trap can be formed at $(0, z_0)$. When $B_{bias} = -0.028\mu_0J_c$ a quadrupole trap is formed at $z_0 \sim 0.7a$, as shown in Fig.8(a). For small bias fields, increasing the magnitude of B_{bias} reduces the trap distance to the chip surface. When $|B_{bias}| \sim 0.06\mu_0J_c$, the quadrupole trap transforms into a ring trap, as shown in Fig.8(b). Further increasing the bias field will enlarge the radius of the ring trap until the trap is lowered to the surface. Alternatively, a ring trap may be formed by applying two field pulses and a bias field as indicated in Fig.9. The first pulse has a magnitude of μ_0J_c , the second has a magnitude of $-0.5\mu_0J_c$ and the bias field $B_{bias} = 0.005\mu_0J_c$. The ring trap of Fig.9 has a larger radius and distance to the surface as well as tighter confinement than the one shown in Fig.8(b).

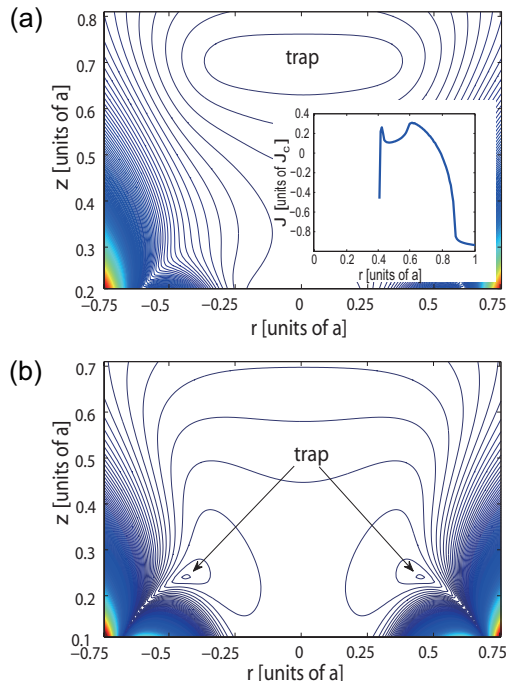


FIG. 8: (Color online) (a) A quadrupole trap formed by a loading field pulse $B_{ext} = 0 \rightarrow 0.8\mu_0J_c \rightarrow 0$ and a bias field $B_{bias} = -0.028\mu_0J_c$. The field variation per contour line is $2 \times 10^{-3}\mu_0J_c$. Inset: Distribution of the sheet current density along the radial direction of the superconducting ring. (b) A ring trap formed when increasing the bias field to $B_{bias} = -0.06\mu_0J_c$. The field variation per contour line is $5 \times 10^{-3}\mu_0J_c$.

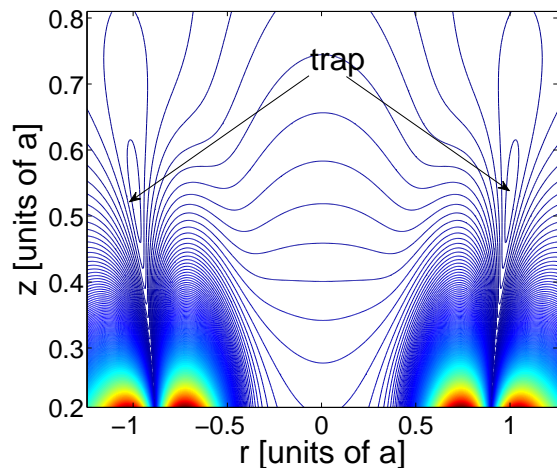


FIG. 9: (Color online) A ring trap formed by a loading field sequence $B_{ext} = 0 \rightarrow \mu_0J_c \rightarrow -0.5\mu_0J_c \rightarrow 0$ and a bias field $B_{bias} = 0.005\mu_0J_c$. The double pulse sequence increases the confinement of the atoms in the ring compared to the single pulse loading sequence. The field variation per contour line is $1.8 \times 10^{-3}\mu_0J_c$.

IV. Conclusion

We have investigated and designed a variety of confining geometries for ultra cold neutral atoms based on type-II superconducting disk and ring structures. These geometries include quadrupole traps, a self-sufficient trap and ring traps. We have shown that a quadrupole trap above a superconducting disk and ring can be formed by applying a single magnetic field loading pulse and adding an external bias field. Using a double pulse sequence we are able to produce a self-sufficient trap above the disk center. We have developed a procedure for the formation of ring traps based on superconducting disk and ring structures. Furthermore we have shown an efficient loading procedure for these ring traps. Apart from methods outlined in this paper based on superconductors in the mixed state, it is possible to produce quadrupole traps with a ring-shaped superconductor in the Meissner state using flux trapped inside the ring and a bias field. By varying the trapped flux and bias field magnitudes ring traps can be produced. However, the limitations on the imprinted current distribution make it impossible to generate versatile magnetic field patterns [31]. The key point of using type-II superconducting structures is that a single microstructured element is capable of generating tailored complex trap geometries for a variety of experimental implementations. This allows us to control the geometry of confining potentials and their parameters without having to fabricate a new atom chip. In addition to this flexibility, superconductors have the intrinsic

advantage of a low trap loss rate due to the reduced spin flips of the atoms close to the chip surface. The potential contribution to the spin flip rate by vortex motion in the superconductor has yet to be experimentally investigated.

An additional control over the trap geometries, complementary to the magnetic field pulses, can be obtained by dressing the atomic states with a radio-frequency field [32, 33]. This can help to lift the magnetic field zero intrinsically present in quadrupole traps, thus reducing the Majorana spin flip rate. The low field noise in the proposed ring traps may make them an attractive candidate for the construction of a Sagnac-type interferometer [34]. A persistent flow of ultracold atoms, even an analog of the superconducting quantum interference device (SQUID), may be realized in these ring traps [35, 36]. Taking into account all the intrinsic advantages discussed highlights the potential of magnetic traps for neutral atoms based on patterned vortex distributions in superconducting disks and rings.

Acknowledgments

We acknowledge financial support from Nanyang Technological University (grant no. WBS M58110036), A-Star (grant no. SERC 072 101 0035 and WBS R-144-000-189-305) and the Centre for Quantum Technologies, Singapore. We thank S.A. Cheong for fruitful discussion.

-
- [1] D. Cano, B. Kasch, H. Hattermann, D. Koelle, R. Kleiner, C. Zimmermann, and J. Fortágh, *Phys. Rev. A* **77**, 063408 (2008).
 - [2] D. Cano, B. Kasch, H. Hattermann, R. Kleiner, C. Zimmermann, D. Koelle, and J. Fortágh, *Phys. Rev. Lett.* **101**, 183006 (2008).
 - [3] A. Emmert, A. Lupaşcu, M. Brune, J.-M. Raimond, S. Haroche, and G. Nogues, *Phys. Rev. A* **80**, 061604(R) (2009).
 - [4] T. Mukai, C. Hufnagel, A. Kasper, T. Meno, A. Tsukada, K. Semba, and F. Shimizu, *Phys. Rev. Lett.* **98**, 260407 (2007).
 - [5] T. Nirrengarten, A. Qarry, C. Roux, A. Emmert, G. Nogues, M. Brune, J.-M. Raimond, and S. Haroche, *Phys. Rev. Lett.* **97**, 200405 (2006).
 - [6] C. Roux, A. Emmert, A. Lupaşcu, T. Nirrengarten, G. Nogues, M. Brune, J.-M. Raimond, and S. Haroche, *Eur. Phys. Lett.* **81**, 56004 (2008).
 - [7] S. Scheel, P. K. Rekdal, P. L. Knight, and E. A. Hinds, *Phys. Rev. A* **72**, 042901 (2005).
 - [8] B.-S. K. Skagerstam, U. Hohenester, A. Eiguren, and P. K. Rekdal, *Phys. Rev. Lett.* **97**, 070401 (2006).
 - [9] U. Hohenester, A. Eiguren, S. Scheel, and E. A. Hinds, *Phys. Rev. A* **76** (2007).
 - [10] G. Nogues, C. Roux, T. Nirrengarten, A. Lupaşcu, A. Emmert, M. Brune, J. M. Raimond, S. Haroche, B. Plaçais, and J.-J. Greffet, *Europhys. Lett.* **87**, 13002 (2009).
 - [11] C. Hufnagel, T. Mukai, and F. Shimizu, *Phys. Rev. A* **79**, 053641 (2009).
 - [12] B. Kasch, H. Hattermann, D. Cano, T. E. Judd, S. Scheel, C. Zimmermann, R. Kleiner, D. Kölle, and J. Fortágh, *New. J. Phys.* **12**, 065024 (2010).
 - [13] A. Emmert, A. Lupaşcu, G. Nogues, M. Brune, J.-M. Raimond, and S. Haroche, *Eur. Phys. J. D* **51**, 173 (2009).
 - [14] R. Fermani, T. Müller, B. Zhang, M. J. Lim, and R. Dumke, *J. Phys. B* (2010), **43**, 095002 (2010).
 - [15] L. Tian, P. Rabl, R. Blatt, and P. Zoller, *Phys. Rev. Lett.* **92**, 247902 (2004).
 - [16] A. André, D. DeMille, J. M. Doyle, M. D. Lukin, S. E. Maxwell, P. Rabl, R. J. Schoelkopf, and P. Zoller, *Nature Phys.* **2**, 636 (2006).
 - [17] K. Tordrup and K. Mølmer, *Phys. Rev. A* **77**, 020301(R) (2008).
 - [18] J. Verdú, H. Zoubi, Ch. Koller, J. Majer, H. Ritsch, and J. Schmiedmayer, *Phys. Rev. Lett.* **103**, 043603 (2009).
 - [19] A. S. Sørensen, C. H. van der Wal, L. I. Childress, and M. D. Lukin, *Phys. Rev. Lett.* **92**, 063601 (2004).
 - [20] S. Scheel, R. Fermani, and E. A. Hinds, *Phys. Rev. A* **75**, 064901 (2007).
 - [21] F. Shimizu, C. Hufnagel, and T. Mukai, *Phys. Rev. Lett.*

- 103**, 253002 (2009).
- [22] B. Zhang, R. Fermani, T. Müller, M. J. Lim, and R. Dumke, *Phys. Rev. A* **81**, 063408 (2010).
- [23] T. Müller, B. Zhang, R. Fermani, K. S. Chan, Z. W. Wang, C. B. Zhang, M. J. Lim, and R. Dumke, *New. J. Phys.* **12**, 043016 (2010).
- [24] T. Müller, B. Zhang, R. Fermani, K. S. Chan, Z. W. Wang, C. B. Zhang, M. J. Lim, and R. Dumke, *Phys. Rev. A* **81**, 053624 (2010).
- [25] A. A. Abrikosov, *Rev. Mod. Phys.* **76**, 975 (2004).
- [26] E. H. Brandt, *Phys. Rev. B* **50**, 4034 (1994).
- [27] E. H. Brandt, *Phys. Rev. B* **52**, 15442 (1995).
- [28] E. H. Brandt, *Physical Review B* **59**, 3369 (1999).
- [29] G. Blatter, M. V. Feigel'man, V. B. Geshkenbein, A. I. Larkin, and V. M. Vinokur, *Reviews of Modern Physics* **66**, 1125 (1994).
- [30] C. Bean, *Rev. Mod. Phys.* **36** (1964).
- [31] E. H. Brandt and J. R. Clem, *Physical Review B* **69**, 184509 (2004).
- [32] S. Hofferberth, I. Lesanovsky, B. Fischer, J. Verdu, and J. Schmiedmayer, *Nature Physics* **2**, 710 (2006).
- [33] T. Fernholz, R. Gerritsma, P. Krger, and R. J. C. Spreeuw, *Physical Review A* **75**, 063406 (2007).
- [34] A. S. Arnold, C. S. Garvie, and E. Riis, *Phys. Rev. A* **73**, 041606 (2006).
- [35] C. Ryu, M. F. Andersen, P. Cladé, V. Natarajan, K. Helmerson, and W. D. Phillips, *Phys. Rev. Lett.* **99**, 260401 (2007).
- [36] A. Ramanathan, K. C. Wright, S. R. Muniz, M. Zelan, W. T. Hill, C. J. Lobb, K. Helmerson, W. D. Phillips, and G. K. Campbell, *Phys. Rev. Lett.* **106**, 130401 (2011).